

Optimization of Biomethane Production in Mono-Cardboard Digestion: Key Parameters Influence, Batch Test Kinetic Evaluation, and DOM Indicators Variation

Dunjie Li,^{†,||} Liuying Song,^{†,||} Hongli Fang,[†] Yue Teng,[‡] Hongfei Cui,[†] Yu-You Li,[§] Rutao Liu,[†] and Qigui Niu^{*,†,||}

[†]School of Environmental Science and Engineering, China-America CRC for Environment & Health, Shandong University, 72# Jimo Binhai Road, Qingdao 266237, Shandong, P. R. China

[‡]Jiangsu Key Laboratory of Anaerobic Biotechnology, Jiangnan University, Wuxi 214122, P. R. China

[§]Department of Civil and Environmental Engineering, Graduate School of Engineering, Tohoku University, 6-6-06 Aoba, Aramaki, Aoba-ku, Sendai 980-8579, Japan

Supporting Information

ABSTRACT: Mono-cardboard waste digestion in batch tests associated with different impact factors was investigated. The maximum methane generation was 394 mL/gVS_{add} with the best F/M of 0.5 at mesophilic conditions. The highest methane content reached 75% in the dynamic water bath feeding with an average particle size of 1–3 mm. Hydrolysis and methanogenesis were significantly different between static and dynamic states, especially at particle size over 3 mm. The modified Gompertz model ($R^2 > 0.98$) and the modified Aiba model ($R^2 > 0.88$) were the most appropriate models for methane generation among the six kinds of models. At different TS, the variation of dissolved organic matters reflects the metabolic rate of the microbial community. The soluble microbial product-like and protein-like components half split by excitation–emission matrix-parallel factors significantly negatively corresponded to biomethane production. Moreover, a rapid loss of methanogenesis was observed with high organics concentration. A strong correlation between the F/M ratio and the CH₄ generation ability was observed with an optimized F/M of 0.5. The maximum energy production was also investigated based on the optimized particle size of 2–5 mm and F/M of 0.5, in which long-term stability was maintained.

1. INTRODUCTION

The rapidly developing e-commerce in China, especially the huge amount of cardboard produced by express business has caused environmental issues. There were 4 billion boxes used for express in 2017. Particularly, 2 billion cardboards were generated by the business.¹ Traditionally, the cardboard was disposed by burning or landfilling, which could cause secondary pollution impacting the environment and personal health. In addition, paper and cardboard were the major biodegradable organic fractions of municipal solid waste based on the data survey.^{2,3} Understanding the cardboard digestion was essential for the municipal solid waste treatment.

Meanwhile, anaerobic digestion (AD) is considered as one of the most successful technologies commonly employed to stabilize and reduce the organic wastes for sustainable alternative energy recovery (biomethane). Digestion as a sustainable waste management solution for cardboard could be used in a wider range of applications.⁴ The successful digestion application needs to be monitored and controlled to maintain good performance especially for mono-cardboard digestion and on-site digestion system.⁵ Previous studies have mostly focused on the co-digestion with food waste,⁶ adjusting the C/N with other substrates⁷ and the effect of shredding pretreatment.² Also, Ferraro⁸ used to improve biomethane production from lignocellulosic materials by bioaugmentation. However, the contribution of mono-cardboard waste in digestion and its potential for methane generation have

scarcely been reported. In practice, tackling the characteristics of the mono-cardboard digestion is urgently needed for understanding the optimum conditions for waste reduction with energy generation and the potential engineering application.

Moreover, mathematical models were used to observe, predict, simulate, and optimize the system's behavior at different conditions. Practically, response surface methodology facilitates statistical analysis within multidimensional design spaces⁹ and the kinetic models provide the metabolic information for the optimal management of digestion.¹⁰ In addition, to better realize the hydrolysis of the digestion, the dissolved organic matter (DOM) composition and variation were evaluated to reveal the process stability.

Therefore, the main objective of this study is to evaluate the kinetics of biomethane production, and the influence parameters on mono-cardboard digestion, such as the optimized feeding TS, F/M ratios, substrate particles, process operation, temperature shocks, and the C/N. The optimal condition with kinetic parameters of mono-cardboard digestion is crucial for the successful operation. The obtained sustainable waste treatment of mono-cardboard digestion could be a possible commercial application.

Received: February 11, 2019

Revised: April 22, 2019

Published: April 23, 2019



2. METHODOLOGY

2.1. Feedstock and Inoculums. The anaerobic inoculum was obtained from a good condition UASB reactor in this study. Cardboard was taken from packaging case with pretreatment of grinding granularity from 0.1 to 1 cm. Serial batch tests were analyzed with cardboard under different conditions. The characteristics of cardboard and seed sludge are shown in Table 1.

Table 1. Characteristics of Seed Sludge and Cardboard Waste for the Batch Experiments^a

component	seed sludge	cardboard waste
TS	12.94%	93.6%
VS	9.52%	87.6%
COD	0.17 g/g*	1.26 g/g
nitrogen	37.60 mg/g	5 mg/g
TP	33.07 mg/g	4.6 mg/g
C	—	40.7%
H	—	5.22%
O	—	53.06%
N	—	0.38%
S	—	0.65%

^a—: no detection; *: g/g (wet sludge).

2.2. Experimental Design. Design-Expert 8.05 software was used to make a design for the surface response analysis focusing on the TS fraction, temperature (*T*), and substrate C/N. The details of the experiment are described in the Supporting Information. One factor analysis was conducted in a batch vial with an effective volume of 100 mL. Each vial was inoculated by seed sludge with 10 g of NaHCO₃ buffer solution to keep the initial pH around 7.5. Pure nitrogen gas was used for gasifying the oxygen outside the headspace and liquid phase for 25 min. The batch tests were performed by shaking at 120 rpm (except the static digestion) in mesophilic condition at 35 ± 2 °C press-balanced after 5 min warming. Biogas production was measured using a syringe and converted to the standard conditions. The carbon dioxide contents were captured completely by a saturated NaOH solution, with the measured value for biomethane, as described in our previous report.¹¹ The biogas and biomethane were measured following

the reaction and transferred to the standard atmospheric pressure.

2.3. Excitation–Emission Matrix (EEM)-Parallel Factor (PARAFAC) Analysis. Fluorescence EEMs were measured on an F-4600 spectrophotometer (Hitachi, Japan) with emission spectra from 200 to 550 nm at 0.5 nm increments and the excitation wavelengths from 200 to 450 nm at 5 nm increments. The inner-filter effect of fluorescence of each sample was corrected by deducting Milli-Q water blank. The split-half validation was carried out with MATLAB 8.5 (MathWorks, Natick, MA) based on the modified drEEM toolbox protocol.¹²

2.4. Chemical and Statistical Kinetics Simulations. The pH, alkalinity, COD, NH₄⁺, TS, VS, TN, and TP were analyzed according to standard methods.¹³ The C, H, O, N, and S organic elements were measured by an organic elemental (Vario Macro Cube). The methane content was measured by a saturated NaOH solution to capture CO₂. As described in our previous study,¹⁴ free volatile fatty acid (VFA) concentration was calculated according to the equilibrium eq 1

$$\text{free VFA} = \frac{\text{TVFA}}{(1 + 10^{-\text{pK}_a + \text{pH}})} \quad (1)$$

where free VFA = free VFA concentration (mg/L); TVFA = total VFA concentration (mg/L); pK_a = dissociation constants of the individual VFAs, with values of 4.757, 4.874, 4.812, and 4.835 for acetic, propionic, butyric, and valeric acids at 25 °C, respectively.

The biogas and biomethane were simulated using a modification of the first-order kinetics¹⁵ (eq 2), the modified Gompertz model¹⁶ (eq 3), the Fitzhugh model¹⁷ (eq 4), the cone model¹⁸ (eq 5), the transference model¹⁹ (eq 6), and the modified second-order model²⁰ (eq 7), which can be written as

$$G(t) = \frac{dM(t)}{dt} = B_0(1 - \exp(-K_{\text{max}}t)) \quad (2)$$

$$G(t) = \frac{dM(t)}{dt} = B_0 \exp\left[\frac{K_{\text{max}}e}{B_0}(\lambda - t) + 1\right] \quad (3)$$

$$G(t) = \frac{dM(t)}{dt} = B_0(1 - \exp(-K_{\text{max}}t)^n) \quad (4)$$

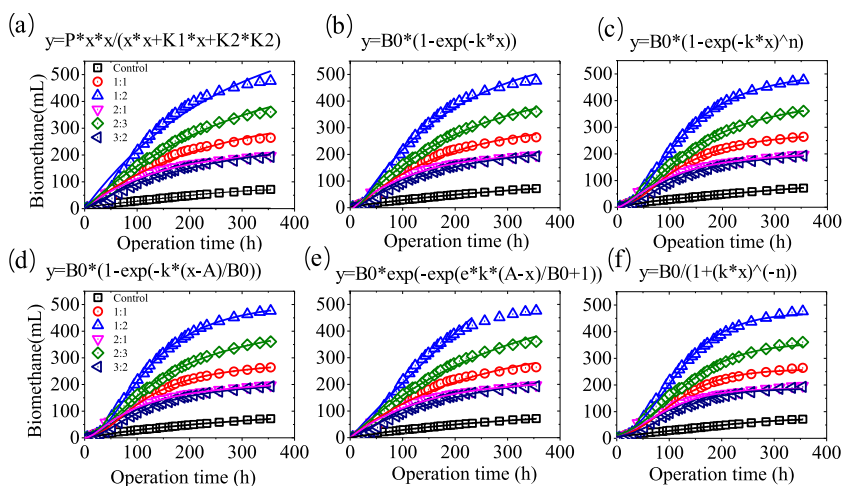


Figure 1. Simulation of bio-CH₄ yield at different F/M ratios by six kinetic models.

Table 2. Kinetic Simulation of Different Models for Biogas and Biomethane at Individual F/M

F/M	biogas					biomethane						
	control	1	0.5	2	0.66	1.5	control	1	0.5	2	0.66	1.5
$y = B_0(1 - \exp(-kx))$	B_0	158.19	446.51	770.06	282.46	600.06	118.47	319.25	599.68	208.42	462.57	227.28
	k	0.41	2.54	4.57	1.58	3.22	0.30	1.85	3.20	1.71	2.22	1.36
$P \exp(-\exp(K \times 2.72(A - x)/P + 1))$	A	-6.62	12.83	15.00	12.53	12.68	-9.39	12.46	15.24	6.39	12.66	12.24
	B_0	118.47	405.96	685.01	256.72	564.94	118.47	294.19	532.38	224.09	442.36	215.41
	k	0.00	0.01	0.01	0.01	0.01	0.00	0.01	0.01	0.01	0.01	0.01
$y = B_0/(1 + (kx)^{-n})$	A	0.81	2.00	2.18	1.97	1.80	0.73	1.96	2.05	1.49	1.68	1.85
	B_0	142.20	497.50	871.70	314.69	675.51	102.18	353.66	241.66	215.89	531.62	251.10
	k	0.57	1.10	0.13	0.00	0.00	1.36	0.34	0.49	0.01	0.01	1.30
	n	0.01	0.00	0.03	1.01	9.96	0.00	0.01	0.00	0.67	0.38	0.00
$y = B_0(1 - \exp(-kx)^n)$	B_0	106.37	360.31	621.42	226.74	480.52	106.37	360.31	621.42	226.74	480.52	262.12
	k	0.33	2.11	3.90	1.32	2.60	0.33	2.11	3.90	1.32	2.60	1.54
$y = P_{ex}/(xx + K_1x + K_2K_2)$	A	-10.50	21.69	26.04	21.17	18.71	-10.50	21.69	26.04	21.17	18.71	20.42
	P	229.54	402.75	652.71	258.20	603.79	162.35	296.21	524.70	246.13	499.20	226.74
	K_1	495.11	-2.87	-30.25	4.38	48.42	458.82	6.34	-10.16	78.90	96.96	33.50
	K_2	0.00	-117.88	-122.71	-116.73	-111.59	0.00	-114.38	-126.13	-61.29	-110.59	-106.07
$y = B_0(1 - \exp(-kx)^n)$	B_0	142.20	497.50	871.70	314.69	675.51	102.18	353.66	2418.66	215.89	531.62	251.10
	k	0.57	1.10	0.13	0.00	0.00	1.36	0.34	0.49	0.01	0.01	1.30
	n	0.01	0.00	0.03	1.01	9.96	0.00	0.01	0.00	0.67	0.38	0.00

Table 3. Kinetic Simulation of Different Models for Biogas and Biomethane at Different Particle Sizes under Static and Dynamic States

particle size (mm)	biogas in static conditions						biogas in dynamic conditions					
	0	3	0.5	10	0	5	2	1	0.5	10	0.15	10
$y = B_0(1 - \exp(-kx))$	B_0	128.88	484.69	492.36	481.56	194.49	208.48	214.13	251.04	221.58	229.71	168.40
	k	0.00	0.00	0.00	0.00	0.00	0.00	0.00	0.00	0.00	0.00	0.00
$y = B_0 \exp(-\exp(2.73k(A - x)/B_0 + 1))$	B_0	75.25	394.31	396.10	378.06	26.45	141.79	134.91	126.35	114.51	96.05	140.79
	k	0.16	1.27	1.27	1.22	0.64	3.50	3.47	3.02	2.58	2.94	2.96
$y = B_0(1 - \exp(-kx)^n)$	A	-1.08	-3.32	-1.74	2.37	9.22	13.76	12.98	12.63	14.74	10.80	11.71
	B_0	128.89	484.69	492.38	481.58	235.15	210.60	181.20	175.00	242.80	229.82	193.18
	k	0.01	0.06	0.06	0.06	0.01	0.00	0.00	0.00	0.00	0.05	0.00
	n	0.20	0.06	0.06	0.06	0.01	0.00	0.00	0.00	0.00	0.05	0.00
$y = B_0/(1 + (kx)^{-n})$	B_0	422.97	588.76	583.93	535.64	32.32	156.41	148.75	142.53	127.91	103.70	173.14
	k	0.00	0.00	0.00	0.00	0.03	0.03	0.03	0.03	0.03	0.04	0.02
	n	0.90	1.18	1.21	1.28	2.15	2.85	2.82	2.65	2.80	2.85	2.28
$y = B_0(1 - \exp(-k(x - A)/B_0))$	B_0	150.06	476.78	483.11	467.34	104.11						
	k	0.17	1.76	1.74	1.64	0.51	2.32	2.27	2.05	1.77	1.76	2.16
	A	-7.80	2.61	2.95	4.50	3.26	5.11	4.53	4.56	6.16	1.98	4.54
$y = Pxx/(xx + K_1x + K_2K_2)$	P	202.37	209.88	252.11	236.21	33.93	111.87	112.65	111.88	80.92	85.35	161.06
	K_1	1.91	9.88	1.58	3.78	-1.30	-43.93	-38.52	-35.35	-52.34	-27.06	-18.02
	K_2	0.00	-0.01	0.01	0.00	38.39	-46.97	-44.66	-45.75	-50.31	-36.31	-48.12

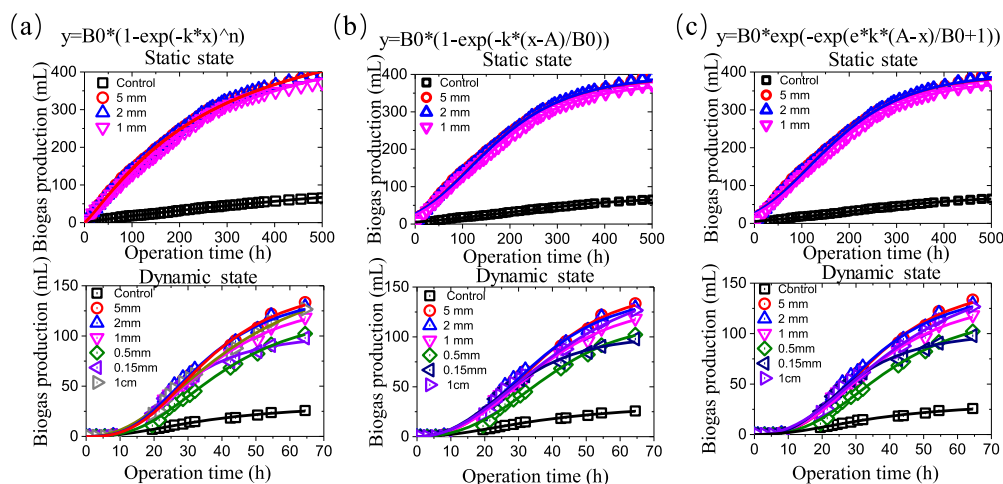


Figure 2. Biogas production simulation at different particle sizes both in static (35 °C of 5, 2, and 1 mm) and dynamic states (35 °C, 120 rpm of 5, 2, 1, 0.5, 0.15 mm, and 1 cm).

$$G(t) = \frac{dM(t)}{dt} = \frac{B_0}{1 + (K_{\max}t)^n} \quad (5)$$

$$G(t) = \frac{dM(t)}{dt} = B_0(1 - \exp(-K_{\max}(t - A)/B_0)) \quad (6)$$

$$G(t) = \frac{dM(t)}{dt} = B_0 \times t \times t / (t^2 + K_{\max}t + K_{\max_2}K_{\max_2}) \quad (7)$$

where G is the methane production rate (mL/gVS/d), B_0 is the biogas or biomethane accumulation concentration (mg/L), K_{\max} is the maximum biogas (biomethane) accumulation rate; K_{\max_2} is the maximum removal rate of two-phase model; λ is defined as the x -axis intercept of this tangent (mg/L); and n is the shape factor.

The methane production rate at t_{\max} eq 3 was obtained when G achieves K_{\max} (at t_{\max} point), which can be calculated as

$$t_{\max} = \lambda + \frac{P}{K_{\max}e} \quad (8)$$

3. RESULTS AND DISCUSSION

3.1. Batch Performance and Kinetic Analysis.

3.1.1. Mesophilic Methane Production at Different Food-to-Microorganism Ratio (F/M). The cumulative biogas and biomethane production of each batch test was measured in individual regular patterns (Figures 1 and S1). The control batch test showed that less than 100 mL of biogas were generated. However, at an F/M of 0.5, a maximal biogas production of 650 mL was obtained with a methane content of 69%, which was 5.8 times higher than the control. The maximum biogas and biomethane yields were 621 and 476 mL, respectively. Additionally, the high F/M led a low biogas and biomethane production with a gradual decrease followed by the F/M ratio increase. Particularly, at the F/M ratio from 1 to 2, the biogas yield remained around 200 mL, which was less than half compared to an F/M of 0.5. Similar results of a large inoculum amount allowed successful digestion in a batch process without pH adjustment in the assessment of the biomethane potential production.²¹ However, at an F/M of 1.5, the biogas and biomethane yields were decreased to 269 and 197 mL, respectively. Meanwhile, the F/M increased up to

2, resulting in biomethane yield even lower than 190 mL (Figure 1). High F/M means that the quantitative microorganisms were subjected to high organic loads and even exceed the microorganisms handling capacity, which could cause the failure of digestion (Figure S2). Moreover, the decreased trend in this study was consistent with previous findings that high F/M exceeds the consumption capacity of the inoculum in the system.²² Subsequently, the kinetic analysis had indicated that there is a demarcation point at F/M of 0.5 (Table 2). The maximum methane potential B_0 estimated by the five models showed a downward trend from F/M of 0.5 to F/M of 2. This observation was in line with the previous study by Hamza,²³ who found that the favorite F/M ratio of 0.5–1.0 gCOD/gSS was beneficial to the stable long-term granule stability, but methane production showed a downward trend over the optimal ratio. Meanwhile, the lag phase times of all of the experiments were short even with the longest time of 2 h at the F/M of 0.5. This indicated that the sludge had a high activity and the mono-cardboard has high biodegradability. Moreover, the methane production t_{\max} was found in two peaks, the first peak was found at the time of 75 h for most tests since the degradable organic matters in the substrate were converted into methane, while the second peak was found at 275 h with the gradual methanogenesis followed the hydrolysis (Figure S2). The multipeak of t_{\max} revealed that the hydrolysis is the rate-limited step in the digestion, and the capacity of methanogenesis was high with a well-worked metabolic network.

It is worth mentioning that a strong correlation was found between the F/M ratio and biomethane production (Figure 1 and Table 2). The results indicated that the high F/M was not feasible for the methanogenesis of cardboard digestion. The inappropriate substrate to inoculum ratio led to the excessive production of organic matter, which was immediately transformed into VFAs in the acidogenesis phase causing inhibition.^{24,25} Therefore, based on the experiment, the optimized F/M was suggested to be 0.5 in the mono-digestion of cardboard.

3.1.2. Mesophilic Methane Production at Different Particle Sizes. The particle size was closely related to hydrolysis,²⁶ especially for the high molecular compound biodegradation for avoiding both the substantial mechanical problems and energy consumption.²⁷ In this study, different

Table 4. Kinetic Simulation of Different Models for Biogas and Biomethane at Different TS Feeding

	TS (%)	0.5	2.5	5	10	30	20	
$y = B_0(1 - \exp(-kx))$	B_0	136.71	120.41	120.00	114.43	98.67	102.72	
	k	0.008	0.01	0.011	0.013	0.013	0.012	
$y = B_0(1 - \exp(-kx)^n)$	B_0	136.71	120.41	120.00	114.43	98.67	102.72	
	k	0.09	0.10	0.11	0.11	0.11	0.11	
	n	0.09	0.10	0.11	0.11	0.11	0.11	
$y = B_0/(1 + (kx)^{-n})$	B_0	126.77	172.63	158.48	128.08	157.92	130.14	
	k	0.01	0.01	0.01	0.02	0.01	0.01	
	n	1.86	0.95	1.00	1.30	0.79	1.06	
	B_0	130.84	122.77	121.54	114.29	101.57	103.76	
$y = B_0(1 - \exp(-k(x - A)/B_0))$	k	1.26	1.17	1.36	1.52	1.16	1.21	
	A	5.80	-3.15	-2.45	0.25	-5.59	-1.91	
	$P \exp(-\exp(K \times 2.72 \times (A - x)/P + 1))$	P	113.04	112.65	113.90	107.26	95.97	97.02
	K	1.01	0.75	0.84	0.97	0.68	0.76	
$y = Pxx/(xx + K_1x + K_2K_2)$	A	10.65	-10.45	-10.08	-3.70	-16.67	-8.77	
	P	201.27	164.25	159.08	150.29	126.93	135.73	
	K_1	165.99	114.31	93.63	83.43	78.47	90.17	
	K_2	0.00	0.00	0.00	0.00	0.00	0.00	

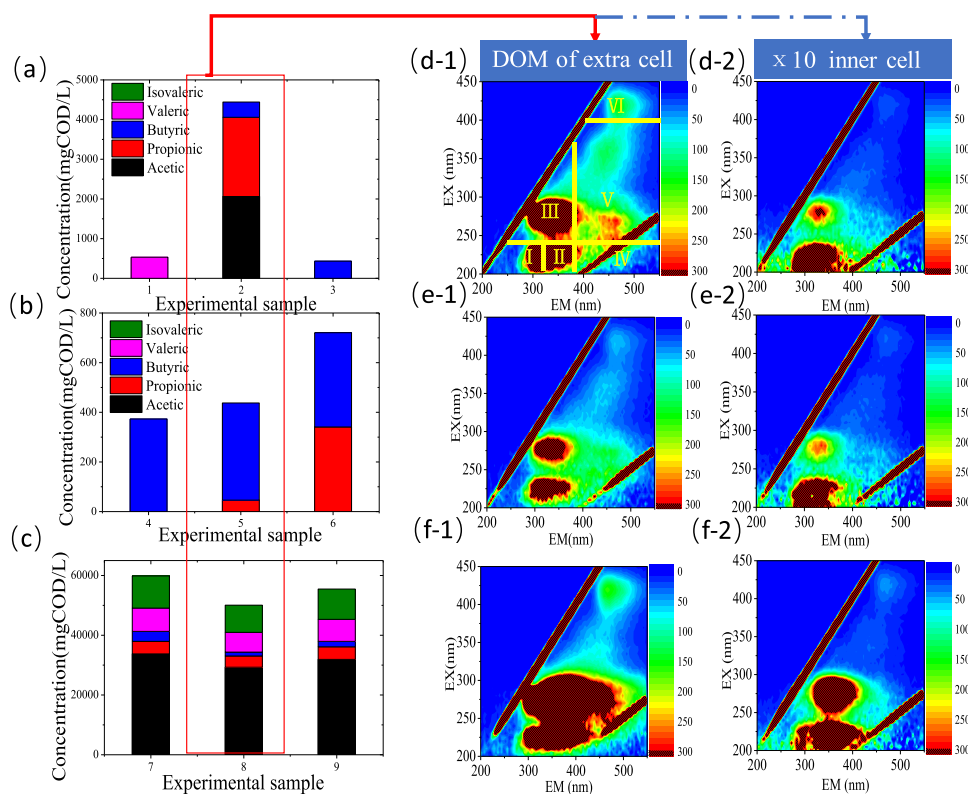


Figure 3. Batch experiment performance of VFA analysis at 15 °C (a), 35 °C (b), 55 °C (c), DOM analyzed of extra and inner cell (d–f) by EEM.

particle sizes in batch tests in both static and dynamic states were conducted to investigate biomethane production (Table 3). Significantly, the substrate particle size was more critical in the dynamic state than in the static state, which was mainly dominated by energy consumption and biomass transfer. In the dynamic state, the mass transfer was faster than in the static state due to the particle size reduction.^{28,29} Although, it was hypothesized that small particles increased the available surface area of digestive enzymes, while larger particles led to longer transit time of absorption and metabolism. Zhang³⁰ also pointed out that the utilization rate of the maximum substrate was doubled when the average particle size of FW decreased from 2.14 to 1.02 mm, more specifically, cellulolytic enzymes

were important for the breakdown of cardboard.³¹ Interestingly, the results showed that there was no significant trend between the static and dynamic states. The particle size between 0.5 and 3 mm in static conditions and between 2 and 5 mm in dynamic conditions all obtained high methane generation (Figures 2 and S3). According to their research, the maximum cumulative methane production was obtained at the particle size of 0.6 mm. Consequently, the particle sizes below 1 cm had a positive effect on the rate of VS reduction, accompanied by an increase in the total production of VFAs.

3.1.3. Thermophilic Methane Production at Different TS. To investigate the optimal TS of feeding, a series of TS were used for the kinetic evaluation (Table 4). Concerning the

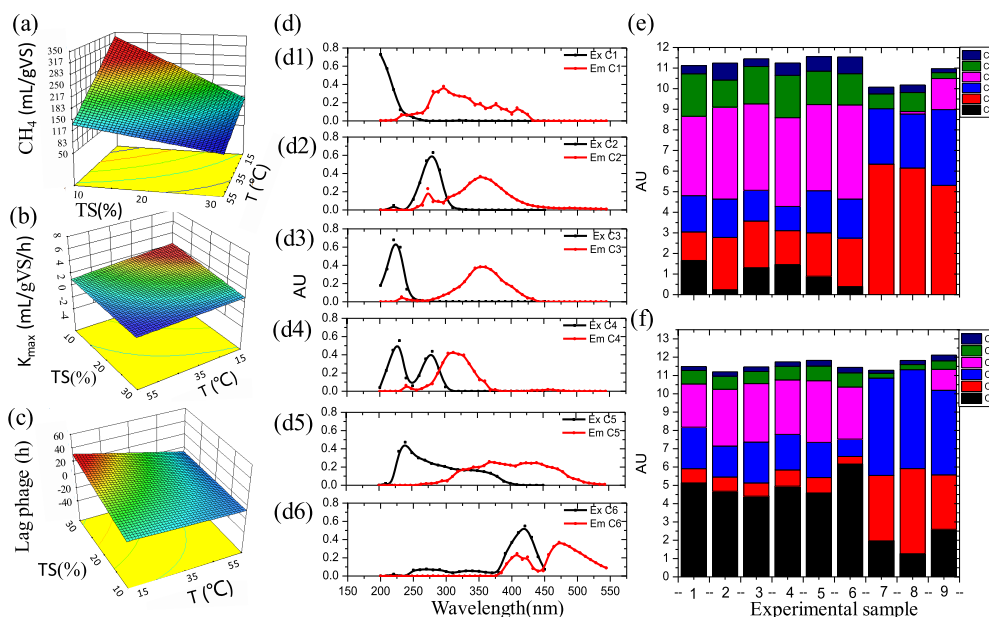


Figure 4. Response surface curve of the relationship between TS, T, and C/N (a–c); EEM-PARAFAC (d) of extra cell DOM (e) and inner cell DOM (f) variation.

stability of digesters, pH values were stable (6.8–7.5). Except for the modified 1 order model (eq 7), the other simulated models obtained a high fitting rate with the R^2 over 0.97. The first-order kinetics model (eq 2), the modified Gompertz model (eq 3), and the Fitzhugh model (eq 4) fitted the result well with R^2 of 0.997, 0.95, and 0.993, respectively. The highest simulated K_{max} of different feeding were all obtained at TS of 10% with 0.013 of the first-order kinetics, 0.11 of the Fitzhugh model, 0.02 of the Cone model, 1.52 of the Transference model, and 0.97 of the modified Gompertz model. For the Transference model and the modified Gompertz model, there was no obvious lag phase on the TS adding. Evaluation of the kinetic models' results suggested that the hydrolysis constant (k) may not be a universal constant because it is specifically calculated for a given sample under certain conditions.

High TS significantly decreased the biomethane yield and the production rate (Table 4), since the low available water concentration could affect the microbial mobility or nutrients and enzymes transport. Moreover, among the composition of cardboard, cellulose and hemicellulose are fermentable after hydrolysis, but lignocellulosic biomass was resistant to degradation by microbes. The accumulation of digestion intermediates, such as ammonia and volatile fatty acids (VFAs), may lead to system instability. The low water contents could slow the mass transfer between the inoculum or feedstock and decreased the mass transfer about 60% when TS increased from 20 to 30%.^{32,33} The inhibited biomethane at high TS in this study agreed with previous studies of batch AD, which amended with 14% TS.³⁴ In this study, the degradable properties of the organic compositions were required to be less than the TS of 10%.

3.2. Response Surface Analysis of the Impactor Factor of TS, T, and C/N. **3.2.1. Methane Production and Kinetic Analysis.** Three central impacted factors, TS, temperature, and C/N, in batch experiment were selected to generate the response surface curve for mono-cardboard digestion (Figures 3 and 4). The performance of VFA analysis is shown at 15 °C (Figure 3a), 35 °C (Figure 3b), and 55 °C (Figure

3c) with the EEM variation. More information can be found in Figures S4 and S5. While at the fixed C/N of the initial experiment without nitrogen addition, the biomethane production increased with the increase of T. The highest biomethane appeared at 55 °C and a TS of 10% (Figure 4). Moreover, according to this diagram at a C/N of 75, the optimum biomethane production was achieved at a TS of 10% at 55 °C and a TS of 30% at 15 °C; however, the increased C/N of 150 shows the opposite result, i.e., optimum biomethane production at a TS of 30% and 15 °C. This phenomenon may explain that there was more free ammonia in the system at high temperature (T) causing inhibition. The relationship between C/N and T showed a gentle positive effect of T on the methane generation both at the TS of 10 and 20%, but a significant difference at a TS of 30%. However, the TS was changed to 30%, and without this effect, the methane production increased significantly with increasing C/N at 15 °C. Our results showed low TS digestion due to high biomethane production (Figure 4a) and K_{max} of biomethane production rate (Figure 4b) even at low temperature. However, the low TS and low T led to a longer lag phase at a fix optimized C/N of 60 (Figure 4c). Response surface methodology was well applied for this study based on the previous study.³⁵

Moreover, the results of this study strongly supported that the temperature shock decreased the activity of methanogens. Even though the microbial community could adapt to the environment, however, a temperature shock could affect microhabitat, making the activity weak, especially for acetogenic methanogens. A similar decrease of the genus and the specific functional genus in activity treatment was reported by Tian.³⁶ The microbe could not afford or resist the shock in such a narrow time; moreover, the activity of microbes that accommodated mesophilic conditions was decreased while transferred to thermophilic conditions directly. In addition, for biomethane production, the terms of C/N and TS showed a significantly positive effect on the production and production rate. The effect of interaction among the TS, C/N, and

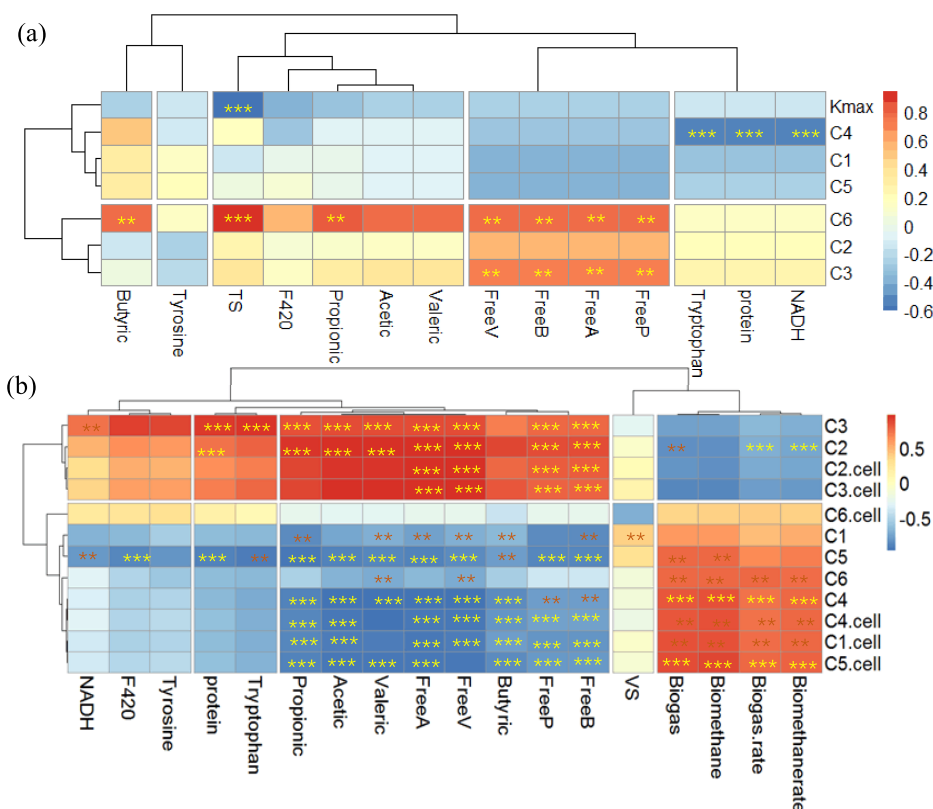


Figure 5. Pearson's correlation analysis between the PARAFAC component and the parameters in different TS digestion (a), and response surface analysis experiment (b). The strength of correlation is defined by a color code with red indicating positive correlation and blue indicating negative correlation (** $p < 0.05$; *** $p < 0.01$).

temperature on the biomethane production can be observed by three-dimensional response surface plots, as shown in Figure 4a. The greatest biomethane generation was observed at a temperature of 35 °C and a TS of 10%. These findings strongly suggested that the synthetic interactions of hydrolysis, acidogenesis, acetogenesis, and methanogenesis took place rapidly and developed a stable conversion rate. This phenomenon was corresponding to the optimization of TS, C/N, and temperature.

Analysis of variance analysis showed that the TS was a significant factor, in addition to the interaction of T and TS. Multivariate statistical analysis in terms of actual factors is described as below in eq 9

$$\begin{aligned}
 B_{\text{CH}_4} = & +597.01916 - 6.53552 \times T - 15.56593 \times \text{TS} \\
 & - 0.88524 \times \text{C/N} + 0.16472 \times T \times \text{TS} \\
 & - 1.14640 \times 10^{-3} \times T \times \text{C/N} + 0.046870 \\
 & \times \text{TS} \times \text{C/N} \quad (9)
 \end{aligned}$$

The effect of TS was higher than T and C/N, while the interaction of TS and C/N was more important than other factors. The K_{max} of biomethane production rate can be described as in eq 10

$$\begin{aligned}
 K_{\text{max}} = & 4.14177 - 0.040708 \times T - 0.11142 \times \text{TS} \\
 & - 6.68247 \times 10^{-3} \times \frac{\text{C}}{\text{N}} + 1.12701 \times 10^{-3} \times T \\
 & \times \text{TS} - 8.22192 \times 10^{-6} \times T \times \text{C/N} \\
 & + 3.38623 \times 10^{-4} \times \text{TS} \times \text{C/N} \quad (10)
 \end{aligned}$$

Similar to CH_4 production, the methane production rate K_{max} had the biggest contribution of TS for single-factor interaction and the most significant interaction of TS and C/N for the two-factor interaction. While referring to the methane production lag phase time, the equation can be described as follows (eq 11)

$$\begin{aligned}
 A = & -24.17144 + 0.20621 \times T + 2.49418 \times \text{TS} \\
 & + 0.10260 \times \text{C/N} - 0.037997 \times T \times \text{TS} \\
 & - 1.73073 \times 10^{-4} \times T \times \text{C/N} - 5.32117 \times 10^{-3} \\
 & \times \text{TS} \times \text{C/N} \quad (11)
 \end{aligned}$$

This response surface study allowed us to establish a rapid method for investigating the effects of temperature (T), substrate TS, and C/N ratio on the methane production.

3.2.2. EEM Variation and Process Indicator. The results of biogas/methane (Figure S4) and VFA-DOM variation in both extracellular and intracellular conditions showed a significant difference among the batch tests (Figure 3). DOM as an important indicator of digestion contains different kinds of soluble matters such as soluble microbial production (SMP), carbohydrates/polysaccharides, amino acids/peptides/proteins, lipids, humiclike substances, and anthropogenic organic pollutants.³⁷ In the present study, the fluorescence peaks were divided into six dominated components (Figure 3d). The components of DOM which were closely associated with hydrolysis and acidogenesis in the digester were described as individual samples by the half-split model, according to a similar previous report.^{38–40}

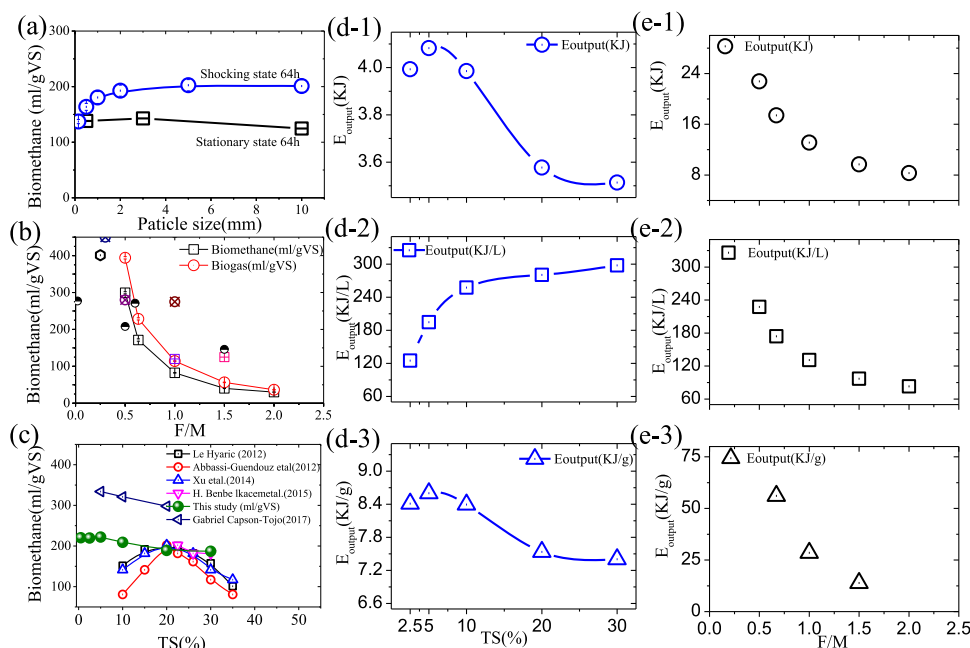


Figure 6. Optimized biomethane production of mono-cardboard digestion particle size (a), F/M (b), TS (c), energy output response to TS (d), and energy output response to F/M (e).

Component 1 (C1) exhibited a primary fluorescence peak at $\lambda_{ex/em} = 220/260$ nm, which can be characterized as tyrosine-like protein. C2 exhibited at $\lambda_{ex/em} = 270/350$ nm were usually defined as SMP-like organics including bio-protein and biological production, while C3 at $\lambda_{ex/em} = 220/350$ nm is usually defined as tryptophan-like aromatic protein. The microbial protein-like component at $\lambda_{ex/em} = 230(280)/280$ nm (C4) shows a mixture peak traditionally defined in ref 41. Component 5 as the humiclike organic matter shows a broad peak at $\lambda_{ex/em} = 250\text{--}400/350\text{--}500$ nm in the limited fluorescence scanning range.^{38,39,42–45} Moreover, C6 had a fluorescence peak at $\lambda_{ex/em} = 420/470$ nm, which was confirmed as a specific enzyme of F420 in the digester.⁴⁶

The PARAFAC components were significantly different in DOM and intercell. In particular, C1 (tyrosine-like) was high in the intercell due to the high content of endoenzyme. The SMP-like (C2) in the batch test under low temperature was higher than that in the batch test under mesophilic condition (Figure S4). However, under thermophilic conditions, the highest content of C2 was observed, even 4 times higher than that at low temperature, while tryptophan-like (C3) and microbial protein-like (C4) have no significant variation among of the tests. Interestingly, in thermophilic conditions, no C4 was detected in test 7 and test 8. It should be pointed out that some non-protein-like fluorophores, including polyphenolic compounds in humiclike substances (e.g., lignin, gallic acid), exhibited the same peak with the critical molecular structure like phenol or aniline.⁴⁷ C4 increased following the biomethane production and decreased since the increase of biomethane production rate. Moreover, the microbial protein-like (C4) is an effective indicator of pollution by artificial human activities and biological metabolites (Figure 4e,f).

Pearson's correlation analysis between the PARAFAC component and the parameters is illustrated in the heatmap (Figure 5). For the TS experiment, the biomethane production rate K_{max} was significantly correlated with TS feeding (Figure 5a), while the DOM component of C4 was correlated with

NADH, protein, and tryptophan at the p level of 0.01. C3 and C6 were significantly correlated with the free VFA at the $p < 0.05$ level. Moreover, C6 also has a significant level of TS at the 0.01 level, followed by propionic and butyric acid.

In contrast, in the batch experiment, the extracellular and intracellular were cultured into two groups with C3, C2, C2 cell, C3 cell having a negative relation to biogas and biomethane (Figure 5b). Free VFA had a significant impact on all of the components at the p level of 0.01. Figure S6 shows that C2 and C3 have a distinctly negative correlation with C1, C4, and C5, whereas C1, C4, and C5 have an obviously positive correlation with each other. C6 only has a significant negative correlation with K_{max} . The above results indicate that C2 and C3 have a common source with C1, C4, and C5, but C6 and another component do not have the same source. Similarly, the TS and VFA have a significant positive correlation with each other, while the NADH, protein, and F420 have no significant correlation with TS and individual VFA. The above results suggest that C2 and C3 are more suitable to assess biodegradability.

3.3. Optimization of the Mono-Cardboard Methane Generation. As described above, the present study investigated the best F/M, particle size, and feeding TS with static and dynamic states for optimized operation conditions. Based on the results (Figure 6), we calculated the thermal energy production of all of the experiment responses to the parameters. Figure 6a shows the net methane generation at different particle sizes within 64 h digestion. In the static running, the biogas production was around 150 mL/gVS of the particle size from 1 to 3 mm but decreased at 1 cm. In contrast, in the dynamic state, a higher biomethane yield of 200 mL/gVS was obtained at a particle size of 2 mm to 1 cm. In contrast, the particle size of 1–2 mm obtained a biomethane from 100 to 150 mL/gVS in the dynamic state. The low biomethane generation at small size agrees with previous studies.^{48,49} Smaller particle size increases the surface area available to the microorganisms, accompanied by increasing

Table 5. Comparison of Biomethane Conversion of Cardboard in the Literature

substrate	co-ratio	digester	F/M	temperature	particle	TS	Y_{CH_4}	refs
cardboard		batch		mesophilic		semi-solid	66 mL/gTVS	(Pena Contreras et al., 2018)
	1.86	batch	0.25	mesophilic		27.50%	409 ± 11 mLCH ₄ /gVS	
food waste: cardboard	1	batch	0.25	mesophilic		27.50%	393 ± 9 mLCH ₄ /gVS	(Capson-Tojo et al., 2018)
	1	batch	0.25	mesophilic		35%	401 ± 16 mLCH ₄ /gVS	
	4	batch	1	mesophilic		27.50%	0 ± 0 mLCH ₄ /gVS	
		batch	0.02	mesophilic	<2 mm	liquid	221 mL/gVS	
corrugated cardboard		batch	0.02	mesophilic	20–100	liquid	272 mL/gVS	(Krause et al., 2017)
		batch	0.02	thermophilic	<2 mm	liquid	188 mL/gVS	
		batch	0.02	thermophilic	20–100	liquid	171 mL/gVS	
dirty paper		batch	0.5	mesophilic		liquid	372 mLCH ₄ /gVS	(Naroznova et al., 2016)
		batch	0.6	mesophilic		liquid	271 mLCH ₄ /gVS	
office paper				thermophilic		liquid	318.3 mL/g substrate	(Prokudina et al., 2016)
paper mixture				thermophilic		liquid	96.6 mL/g substrate	
treated filter paper		batch		mesophilic		liquid	277 ± 25 mLCH ₄ /gVS	
treated office paper		batch		mesophilic		liquid	287 ± 14 mLCH ₄ /gVS	
treated newspaper		batch		mesophilic		liquid	192 ± 17 mLCH ₄ /gVS	
treated cardboard		batch		mesophilic		liquid	231 ± 28 mLCH ₄ /gVS	(Yuan et al., 2012)
untreated filter paper		batch		mesophilic		liquid	214 ± 13 mLCH ₄ /gVS	
untreated office paper		batch		mesophilic		liquid	208 ± 9 mLCH ₄ /gVS	
untreated newspaper		batch		mesophilic		liquid	75 ± 6 mLCH ₄ /gVS	
untreated cardboard		batch		mesophilic		liquid	96 ± 11 mLCH ₄ /gVS	
office paper		batch		thermophilic		liquid	281.8 mLCH ₄ /g substrate	
cardboard		batch		thermophilic		liquid	252.43 mLCH ₄ /g substrate	(Tsavkelova et al., 2012)
office paper		batch		mesophilic		liquid	245.5 mLCH ₄ /g substrate	
cardboard		batch		mesophilic		liquid	240.88 mLCH ₄ /g substrate	
cardboard		batch	batch	mesophilic		liquid	272.8 ± 7.9 mL/gVS fed	(Guo et al., 2011)
cardboard waste		batch	batch	mesophilic		liquid	208 ± 16 mLCH ₄ /gVS	(Sell et al., 2011)
		batch		mesophilic	100 mm	liquid	132 mLCH ₄ /gDM	
paper and cardboard		batch		mesophilic	20 mm	liquid	143 mLCH ₄ /gDM	(Pommier et al., 2010)
		batch		mesophilic	<1 mm	liquid	155 mLCH ₄ /gDM	
cardboard		batch	1.5	mesophilic		liquid	146 ± 25 m ³ /t waste	
newsprint		batch	1.5	mesophilic		liquid	34 ± 6.1 m ³ /t waste	(Jokela et al., 2005)
office paper		batch	1.5	mesophilic		liquid	243 ± 18 m ³ /t waste	
cardboard 1			0.5		0.5	10%	310 ± 25 mL/gVS	
cardboard 2		batch	1	mesophilic			100 ± 25 mL/gVS	this study
cardboard 3			2		10	10%	50 ± 25 mL/gVS	

hydrolysis with the production of soluble organic materials like VFAs, resulting in excessive acidification and causing inhibition.⁴⁸ Accordingly, the particle size from 2 mm to 1 cm in the form of dynamic condition exhibited relatively high degradation and biomethane production, since the cardboard easily absorbs water and degrades with utilizable DOM generated.

Figure 6b shows the literature comparison of the methanogen effects of cardboard under different F/M ratios. The maximum methane production (392 mL/gVS) obtained at an F/M ratio of 0.5 in our study was higher than most literature reported values,⁵⁰ while the value was also slightly lower than the result reported in co-digestion of food waste.⁵¹ The mono-cardboard waste digestion could be inoculated with the F/M ratio of 0.5–1 for the engineering application (Table 5), while Figure 6c shows the response of methane production to the TS feeding. Our results strongly supported lower than 10% TS addition obtained high methane production, since low TS and high water content made the hydrolysis easier (Figure 6c). A corrective linear biological uptake rate for the water content between 0 and 80% was investigated on a larger range (no activity at 80% TS, full activity at 0% TS). Similar results of a constant linear decrease of the biologically specific

methanogenic activity between 18 and 35% TS in cellulose digestion was also reported by Le Hyaric.⁵² Meanwhile, the same trend was found in the batch test of cardboard digestion inoculum at a very high F/M of 20⁵³ as well as corn stover as substrate (also in batch tests) at an F/M ratio of 2.⁵⁰

The biomethane achieved a relatively high methane generation with TS lower than 5%, while a significant decrease of methane generation was found when TS increased from 5 to 30%, similarly to the previous report.⁵¹ Benbelkacem et al.⁵⁴ also found a consistent decline in methane production, when TS increased from 5 to 20% during co-digestion with food waste. The results of EEM responded to relative activity, which was inferred from biomethane production and thus confirmed the optimized biomethane production of mono-cardboard digestion. The energy production based on the thermotical calculation is shown in Figure 6d,e. For the TS feeding test, a 5% TS was obtained with the highest energy production of 8.8 kJ/gVS (Figure 6d), while the F/M test suggested that following the F/M increase, the net energy decreased. If the F/M was 0.5, the highest energy production of 70 kJ/gVS was achieved (Figure 6e).

4. CONCLUSIONS

Mono-cardboard digestion was a feasible and promising treatment with methane generation. An appropriate F/M of 0.5 resulted in the highest methane generation and methane production rate with optimized particle size between 0.5 and 3 mm in both static and dynamic states. Both the kinetic model and first model simulated the dynamics of biogas and biomethane production well. The surface response analysis indicated that the T and TS have a significant effect on methane production. Moreover, the EEM-PARAFAC of F420-like C6 had a strong correlation with biomethane production. Statistical modeling revealed no significant difference below the TS of 10% with a maximum net energy production of 8.5 kJ/gVS.

■ ASSOCIATED CONTENT

Supporting Information

The Supporting Information is available free of charge on the ACS Publications website at DOI: 10.1021/acs.energyfuels.9b00423.

Experimental design; simulation of biogas yield at different F/M ratios by six kinetic models (Figure S1); biomethane production rate of F/M (a), particle size (b), response surface analysis experiment (c), and TS(d) (Figure S2), the biogas production simulation at different particle size both in static and dynamic states (Figure S3), the gas production, extra and inner cell EEM of response surface analysis at 15 °C(a), 35 °C(b), 55 °C(c) (Figure S4), response surface plots for the orthogonal experiment (Relationship between impact factors) (Figure S5) and the Pearson's correlation analysis of TS experiment (Figure S6). (PDF)

■ AUTHOR INFORMATION

Corresponding Author

*E-mail: niuqg@sdu.edu.cn.

ORCID

Yu-You Li: 0000-0003-4067-8855

Rutao Liu: 0000-0002-7451-0682

Qigui Niu: 0000-0002-0997-8967

Author Contributions

[†]D.L. and L.S. contributed equally to this work.

Notes

The authors declare no competing financial interest.

■ ACKNOWLEDGMENTS

This study was supported by the National Natural Science Foundation of China (Grant nos. 51608304 and U1806216) and the Young Scholars Program of Shandong University (2018WLJH53). Research Fund of Tianjin Key Laboratory of Aquatic Science and Technology (TJKLAST-ZD-2017-04) and Research Fund of Jiangsu Key Laboratory of Anaerobic Biotechnology (JKLAB201702) also partly supported this work. "The Fundamental Research Funds of Shandong University" and China Postdoctoral Science Foundation (2017M622209) are also acknowledged.

■ REFERENCES

(1) Yi, Y.; Wang, Z.; Wennnersten, R.; Sun, Q. Life Cycle Assessment of Delivery Packages in China. *Energy Procedia* **2017**, *105*, 3711–3719.

(2) Pommier, S.; Llamas, A. M.; Lefebvre, X. Analysis of the outcome of shredding pretreatment on the anaerobic biodegradability of paper and cardboard materials. *Bioresour. Technol.* **2010**, *101*, 463–468.

(3) Capson-Tojo, G.; Trably, E.; Rouez, M.; Crest, M.; Bernet, N.; Steyer, J. P.; Delgenes, J. P.; Escudie, R. Methanosarcina plays a main role during methanogenesis of high-solids food waste and cardboard. *Waste Manage.* **2018**, No. 76.

(4) Mao, C. L.; Feng, Y. Z.; Wang, X. J.; Ren, G. X. Review on research achievements of biogas from anaerobic digestion. *Renewable Sustainable Energy Rev.* **2015**, *45*, 540–555.

(5) Song, L.; Song, Y.; Li, D.; Liu, R.; Niu, Q. The auto fluorescence characteristics, specific activity, and microbial community structure in batch tests of mono-chicken manure digestion. *Waste Manage.* **2019**, *83*, 57–67.

(6) Tsavkelova, E. A.; Egorova, M. A.; Petrova, E. V.; Netrusov, A. I. [Biogas production by microbial communities via decomposition of cellulose and food waste]. *Appl. Biochem. Microbiol.* **2012**, *48*, 377–384.

(7) Capson-Tojo, G.; Trably, E.; Rouez, M.; Crest, M.; Steyer, J. P.; Delgenes, J. P.; Escudie, R. Dry anaerobic digestion of food waste and cardboard at different substrate loads, solid contents and co-digestion proportions. *Bioresour. Technol.* **2017**, *233*, 166–175.

(8) Ferraro, A.; Dottorini, G.; Massini, G.; Mazzurco Miritana, V.; Signorini, A.; Lembo, G.; Fabbicino, M. Combined bioaugmentation with anaerobic ruminal fungi and fermentative bacteria to enhance biogas production from wheat straw and mushroom spent straw. *Bioresour. Technol.* **2018**, *260*, 364–373.

(9) Jiménez, J.; Guardia-Puebla, Y.; Romero-Romero, O.; Cisneros-Ortiz, M. E.; Guerra, G.; Morgan-Sagastume, J. M.; Noyola, A. Methanogenic activity optimization using the response surface methodology, during the anaerobic co-digestion of agriculture and industrial wastes. Microbial community diversity. *Biomass Bioenergy* **2014**, *71*, 84–97.

(10) Niu, Q. G.; Hojo, T.; Qiao, W.; Qiang, H.; Li, Y. Y. Characterization of methanogenesis, acidogenesis and hydrolysis in thermophilic methane fermentation of chicken manure. *Chem. Eng. J.* **2014**, *244*, 587–596.

(11) Song, L.; Li, D.; Cao, X.; Tang, Y.; Liu, R.; Niu, Q.; Li, Y.-Y. Optimizing biomethane production of mesophilic chicken manure and sheep manure digestion: Mono-digestion and co-digestion kinetic investigation, autofluorescence analysis and microbial community assessment. *J. Environ. Manage.* **2019**, *237*, 103–113.

(12) Murphy, K. R.; Stedmon, C. A.; Graeber, D.; Bro, R. Fluorescence spectroscopy and multi-way techniques. PARAFAC. *Anal. Methods* **2013**, *5*, 6557–6566.

(13) Administration, T. S. E. P. *The Water and Wastewater Monitoring Analysis Method Editorial Board. Water and Wastewater Monitoring Analysis Method*, 4th ed.; China Environmental Science Press: Beijing, 2002; pp 38–47.

(14) Niu, Q.; Qiao, W.; Qiang, H.; Hojo, T.; Li, Y.-Y. Mesophilic methane fermentation of chicken manure at a wide range of ammonia concentration: Stability, inhibition and recovery. *Bioresour. Technol.* **2013**, *137*, 358–367.

(15) Bilgili, M. S.; Demir, A.; Varank, G. Evaluation and modeling of biochemical methane potential (BMP) of landfilled solid waste: A pilot scale study. *Bioresour. Technol.* **2009**, *100*, 4976–4980.

(16) Lay, J. J.; Li, Y. Y.; Noike, T. Interaction between homoacetogens and methanogens in lake sediments. *J. Ferment. Bioeng.* **1998**, *86*, 467–471.

(17) Fitzhugh, H. A. Analysis of Growth-Curves and Strategies for Altering Their Shape. *J. Anim. Sci.* **1976**, *42*, 1036–1051.

(18) Syaichurrozi, I.; Sumardiono, S. Predicting kinetic model of biogas production and biodegradability organic materials: biogas production from vinasse at variation of COD/N ratio. *Bioresour. Technol.* **2013**, *149*, 390–397.

(19) Redzwan, G.; Banks, C. The use of a specific function to estimate maximum methane production in a batch-fed anaerobic reactor. *J. Chem. Technol. Biotechnol.* **2004**, *79*, 1174–1178.

- (20) Ma, L.; Selim, H. Predicting atrazine adsorption-desorption in soils: A modified second-order kinetic model. *Water Resour. Res.* **1994**, *30*, 447–456.
- (21) Gunaseelan, V. N. Anaerobic digestion of biomass for methane production: A review. *Biomass Bioenergy* **1997**, *13*, 83–114.
- (22) Wu, D.; Zhang, Z. M.; Yu, Z. D.; Zhu, L. Optimization of F/M ratio for stability of aerobic granular process via quantitative sludge discharge. *Bioresour. Technol.* **2018**, *252*, 150–156.
- (23) AhmedHamza, R.; ZhiyaSheng; TernaIorhemen, O.; SherifZaghloul, M.; HwaTay, J. Impact of food-to-microorganisms ratio on the stability of aerobic granular sludge treating high-strength organic wastewater. *Water Res.* **2018**, *147*, 287–298.
- (24) Vedrenne, F.; Beline, F.; Dabert, P.; Bernet, N. The effect of incubation conditions on the laboratory measurement of the methane producing capacity of livestock measurement wastes. *Bioresour. Technol.* **2008**, *99*, 146–155.
- (25) Lü, F.; Hao, L. P.; Zhu, M.; Shao, L. M.; He, P. J. Initiating methanogenesis of vegetable waste at low inoculum-to-substrate ratio: Importance of spatial separation. *Bioresour. Technol.* **2012**, *105*, 169–173.
- (26) Motte, J. C.; Escudié, R.; Bernet, N.; Delgenes, J. P.; Steyer, J. P.; Dumas, C. Dynamic effect of total solid content, low substrate/inoculum ratio and particle size on solid-state anaerobic digestion. *Bioresour. Technol.* **2013**, *144*, 141–148.
- (27) Wall, D. M.; Straccialini, B.; Allen, E.; Nolan, P.; Herrmann, C.; O'Kiely, P.; Murphy, J. D. Investigation of effect of particle size and rumen fluid addition on specific methane yields of high lignocellulose grass silage. *Bioresour. Technol.* **2015**, *192*, 266–271.
- (28) Crevieu, I.; Carre, B.; Chagneau, A. M.; Gueguen, J.; Melcion, J. P. Effect of particle size of pea (*Pisum sativum* L) flours on the digestion of their proteins in the digestive tract of broilers. *J. Sci. Food Agric.* **1997**, *75*, 217–226.
- (29) Kariyama, I. D.; Zhai, X. D.; Wu, B. X. Influence of mixing on anaerobic digestion efficiency in stirred tank digesters: A review. *Water Res.* **2018**, *143*, 503–517.
- (30) Zhang, C. S.; Su, H. J.; Baeyens, J.; Tan, T. W. Reviewing the anaerobic digestion of food waste for biogas production. *Renewable Sustainable Energy Rev.* **2014**, *38*, 383–392.
- (31) Stolze, Y.; Zakrzewski, M.; Maus, I.; Eikmeyer, F.; Jaenicke, S.; Rottmann, N.; Siebner, C.; Puhler, A.; Schluter, A. Comparative metagenomics of biogas-producing microbial communities from production-scale biogas plants operating under wet or dry fermentation conditions. *Biotechnol. Biofuels* **2015**, *8*, No. 14.
- (32) Forster-Carneiro, T.; Perez, M.; Romero, L. I.; Sales, D. Dry-thermophilic anaerobic digestion of organic fraction of the municipal solid waste: Focusing on the inoculum sources. *Bioresour. Technol.* **2007**, *98*, 3195–3203.
- (33) Yang, L. C.; Xu, F. Q.; Ge, X. M.; Li, Y. B. Challenges and strategies for solid-state anaerobic digestion of lignocellulosic biomass. *Renewable Sustainable Energy Rev.* **2015**, *44*, 824–834.
- (34) Sui, Q.; Meng, X.; Wang, R.; Zhang, J.; Yu, D.; Chen, M.; Wang, Y.; Wei, Y. Effects of endogenous inhibitors on the evolution of antibiotic resistance genes during high solid anaerobic digestion of swine manure. *Bioresour. Technol.* **2018**, *270*, 328–336.
- (35) Bezerra, M. A.; Santelli, R. E.; Oliveira, E. P.; Villar, L. S.; Escalera, L. A. Response surface methodology (RSM) as a tool for optimization in analytical chemistry. *Talanta* **2008**, *76*, 965–977.
- (36) Tian, Z.; Zhang, Y.; Yu, B.; Yang, M. Changes of resistome, mobilome and potential hosts of antibiotic resistance genes during the transformation of anaerobic digestion from mesophilic to thermophilic. *Water Res.* **2016**, *98*, 261–269.
- (37) Yu, G. H.; Luo, Y. H.; Wu, M. J.; Tang, Z.; Liu, D. Y.; Yang, X. M.; Shen, Q. R. PARAFAC modeling of fluorescence excitation-emission spectra for rapid assessment of compost maturity. *Bioresour. Technol.* **2010**, *101*, 8244–8251.
- (38) Li, X. W.; Dai, X. H.; Takahashi, J.; Li, N.; Jin, J. W.; Dai, L. L.; Dong, B. New insight into chemical changes of dissolved organic matter during anaerobic digestion of dewatered sewage sludge using EEM-PARAFAC and two-dimensional FTIR correlation spectroscopy. *Bioresour. Technol.* **2014**, *159*, 412–420.
- (39) Hur, J.; Shin, J.; Kang, M.; Cho, J. Tracking variations in fluorescent-dissolved organic matter in an aerobic submerged membrane bioreactor using excitation-emission matrix spectra combined with parallel factor analysis. *Bioprocess Biosyst. Eng.* **2014**, *37*, 1487–1496.
- (40) Logue, J. B.; Stedmon, C. A.; Kellerman, A. M.; Nielsen, N. J.; Andersson, A. F.; Laudon, H.; Lindstrom, E. S.; Kritzberg, E. S. Experimental insights into the importance of aquatic bacterial community composition to the degradation of dissolved organic matter. *ISME J.* **2016**, *10*, 533–545.
- (41) Coble, P. G. Marine optical biogeochemistry: The chemistry of ocean color. *Chem. Rev.* **2007**, *107*, 402–418.
- (42) Yang, L. Y.; Hur, J.; Zhuang, W. N. Occurrence and behaviors of fluorescence EEM-PARAFAC components in drinking water and wastewater treatment systems and their applications: a review. *Environ. Sci. Pollut. Res.* **2015**, *22*, 6500–6510.
- (43) Maqbool, T.; Quang, V. L.; Cho, J.; Hur, J. Characterizing fluorescent dissolved organic matter in a membrane bioreactor via excitation-emission matrix combined with parallel factor analysis. *Bioresour. Technol.* **2016**, *209*, 31–39.
- (44) Cheng, C.; Zhou, Z.; Pang, H. J.; Zheng, Y.; Chen, L. Y.; Jiang, L. M.; Zhao, X. D. Correlation of microbial community structure with pollutants removal, sludge reduction and sludge characteristics in micro-aerobic side-stream reactor coupled membrane bioreactors under different hydraulic retention times. *Bioresour. Technol.* **2018**, *260*, 177–185.
- (45) Zheng, W.; Lu, F.; Phoungthong, K.; He, P. J. Relationship between anaerobic digestion of biodegradable solid waste and spectral characteristics of the derived liquid digestate. *Bioresour. Technol.* **2014**, *161*, 69–77.
- (46) Dong, F.; Zhao, Q.-B.; Zhao, J.-B.; Sheng, G.-P.; Tang, Y.; Tong, Z.-H.; Yu, H.-Q.; Li, Y.-Y.; Harada, H. Monitoring the restart-up of an upflow anaerobic sludge blanket (UASB) reactor for the treatment of a soybean processing wastewater. *Bioresour. Technol.* **2010**, *101*, 1722–1726.
- (47) Li, W. T.; Xu, Z. X.; Li, A. M.; Wu, W.; Zhou, Q.; Wang, J. N. HPLC/HPSEC-FLD with multi-excitation/emission scan for EEM interpretation and dissolved organic matter analysis. *Water Res.* **2013**, *47*, 1246–1256.
- (48) Mshandete, A.; Bjornsson, L.; Kivaisi, A. K.; Rubindamayugi, M. S. T.; Mattiasson, B. Effect of particle size on biogas yield from sisal fibre waste. *Renewable Energy* **2006**, *31*, 2385–2392.
- (49) Izumi, K.; Okishio, Y. K.; Nagao, N.; Niwa, C.; Yamamoto, S.; Toda, T. Effects of particle size on anaerobic digestion of food waste. *Int. Biodeterior. Biodegrad.* **2010**, *64*, 601–608.
- (50) Xu, F. Q.; Wang, Z. W.; Tang, L.; Li, Y. B. A mass diffusion-based interpretation of the effect of total solids content on solid-state anaerobic digestion of cellulosic biomass. *Bioresour. Technol.* **2014**, *167*, 178–185.
- (51) Capson-Tojo, G.; Rouez, M.; Crest, M.; Trably, E.; Steyer, J. P.; Bernet, N.; Delgenes, J. P.; Escudie, R. Kinetic study of dry anaerobic co-digestion of food waste and cardboard for methane production. *Waste Manage.* **2017**, *69*, 470–479.
- (52) Le Hyaric, R.; Chardin, C.; Benbelkacem, H.; Bollon, J.; Bayard, R.; Escudie, R.; Buffiere, P. Influence of substrate concentration and moisture content on the specific methanogenic activity of dry mesophilic municipal solid waste digestate spiked with propionate. *Bioresour. Technol.* **2011**, *102*, 822–827.
- (53) Abbassi-Guendouz, A.; Brockmann, D.; Trably, E.; Dumas, C.; Delgenes, J. P.; Steyer, J. P.; Escudie, R. Total solids content drives high solid anaerobic digestion via mass transfer limitation. *Bioresour. Technol.* **2012**, *111*, 55–61.
- (54) Benbelkacem, H.; Bollon, J.; Bayard, R.; Escudie, R.; Buffiere, P. Towards optimization of the total solid content in high-solid (dry) municipal solid waste digestion. *Chem. Eng. J.* **2015**, *273*, 261–267.